The localization of low order rational surfaces based on the intermittence parameter in the TJ-II stellarator

B.Ph. van Milligen[1], B.A. Carreras[2,3], L. García[2], C. Hidalgo[1] and the TJ-II Team

[1] National Fusion Laboratory, CIEMAT, Madrid, Spain
[2] Departamento de Física, Universidad Carlos III de Madrid, Leganés, Madrid, Spain
[3] Department of Physics, University of Alaska, Fairbanks, Alaska

Abstract. This work intends to show that the multifractal concept of intermittence can be fruitfully applied to the identification of the radial location of low order rational surfaces inside a magnetically confined plasma. To do so, we make use of Langmuir probe data from a set of experiments in which the rotational transform was scanned dynamically in the TJ-II stellarator. It is shown that up to five rational surfaces can be identified from the data, which is a first in plasma physics, to the best of our knowledge. The effect of the radial electric field on intermittence was also studied using a specific subset of experiments in which the electron density was raised on a shot by shot basis. The observations are contrasted with results from numerical calculations using a resistive Magneto-HydroDynamic model to facilitate interpretation.

1. Introduction

Turbulence of different types is known to contribute significantly to radial transport in magnetically confined plasmas [1]. The radial transport (of particles, heat, and other quantities) is only partly understood in fusion-grade plasmas, which can be described as strongly driven complex systems, far from thermodynamic equilibrium. Thus, improving our understanding of turbulence and finding methods to control it are important and urgent goals on the road to achieving viable fusion energy.

One aspect of turbulence is intermittence. In the present work we make use of the multifractal quantifier of intermittence [2], based on the analysis of the temporal variations of the signal fluctuation amplitude. The goal of this paper is to show that the latter provides interesting and non-trivial information about the nature of fluctuations, the impact of zonal flows and, in some cases, the location of low order rational surfaces of a plasma in a magnetic confinement device. Establishing the precise location of rational surfaces is an important issue in fusion plasma research, as it provides an indirect measurement of (the modification of) the safety factor (q) or rotational transform ($\iota = \iota/2\pi = 1/q$) profile that reflects the magnetic configuration, both imposed externally by the machine operators and modified internally by currents that may flow inside the plasma itself.

The first application of multifractal intermittence to fluctuation measurements in plasmas was reported in [3]. More recently, we explored its use as a means of detecting rational surfaces in a study based on a resistive Magneto-HydroDynamics (MHD) model for turbulence in stellarators. Subsequently, we applied the technique to temperature fluctuation measurements performed at W7-X [4]. It was shown that the intermittence tends to exhibit minima at the location of low order rational surfaces, both in the model and in the experiment. Although the temperature diagnostic at W7-X offered an acceptable radial resolution, we found it was desirable to achieve still better resolution in order to determine the location of the minima with higher precision.

Therefore, in the present work we turn to a set of unique experiments performed some years ago in the TJ-II stellarator [5]. In these experiments, the edge value of the rotational transform profile (and hence the full profile) was scanned dynamically. This extraordinary capacity is a characteristic feature of this 'flexible Heliac' device [6]. The scans were performed in the course of a time interval of 150 ms during a discharge, while internal plasma currents were kept small. Using Langmuir probes placed at a fixed position in the plasma edge region, we could thus detect the impact of the varying rotational transform on the intermittence parameter calculated from potential fluctuations, by causing low-order rational surfaces to move across the probe position. By analyzing the intermittence in time subwindows of 10 ms, the corresponding effective radial resolution achieved in the present work was about 3 mm, this certainly not being the lower limit of the possibilities offered by this technique.

One set of experiments involved 4 rotational transform scans with about 10 discharges for each scan, in which plasma conditions were kept as constant as possible.

The repeated discharges in each scan allowed verifying reproducibility and accumulating statistics to obtain rather accurate values of the intermittence parameter as a function of local rotational transform. When these results were compared to the intermittence produced by the resistive MHD model in similar conditions, very good agreement was obtained. Thus, the locations of 5 low order rational surfaces inside the plasma could be identified.

In a second set of experiments, involving 22 discharges, the rotational transform scan was repeated while the plasma conditions were varied. Over the set of discharges, the line averaged electron density was raised gradually, although it was kept as constant as possible in each individual discharge. As the density was raised, we found that the intermittence at the rational surfaces decreased, while it increased at other locations. A possible explanation is the increased instability drive (due to increased gradients), which would tend to emphasize monofractal properties at the rational surfaces, while simultaneously increasing the generation of zonal flows and the associated mixing (leading to multifractality) away from the rational surfaces. The reduction of intermittence at rational surfaces led to the detection of a new low order rational that had not been identified in the first set of experiments, performed at low density.

In this second set of experiments, the radial electric field was decreasing as the density was raised. Eventually, the plasma performed a confinement transition from electron to ion root. Thus, the two parameters (electric field and density) varied simultaneously, making it hard to disentangle the influence of each quantity on the intermittence parameter. However, the second set of discharges contained a subset of 6 discharges with similar density yet different electric field. By analyzing these discharges separately, we find that an increase of the radial electric field decreases the intermittence at specific rational surfaces. Again, the response of the intermittence to an added electric field is fully consistent with the results of numerical calculations using the resistive MHD model.

Based on this exceptionally clear evidence, we conclude that the intermittence parameter can be used as a diagnostic for identifying the location of some low order rational surfaces under favorable conditions. However, a strong net poloidal rotation may lead to an increase of the measured intermittence, potentially reducing or even obliterating the minima. One may compare this to the effect poloidal rotation has on the experimental determination of auto-correlation [7].

This article is organized as follows: Section 2 discusses the methods we have used for data analysis and the numerical model for turbulence simulation. Section 3 presents the results for the rotational transform scan experiments and their interpretation based on the numerical model. In Section 4 we discuss the results and draw some conclusions.

2. Methods

The experiments discussed here have been performed in TJ-II, a flexible Heliac with toroidal magnetic field $B_T \simeq 1$ T, major radius $R_0 = 1.5$ m and minor radius $a < 0.22$ m [8]. Plasmas can be heated using two Electron Cyclotron Resonance Heating (ECRH) beam lines delivering up to 300 kW each at a frequency of 53.2 GHz (X mode) and two Neutral Beam Injector (NBI) systems (co and counter) with up to 2×700 kW port-through power.

In this section, we briefly describe the tools we used in this study. Section 2.1 describes the probe systems we used. Section 2.2 describes the resistive MHD model used to perform the turbulence calculations. Section 2.3 describes the calculation of the intermittence parameter ($C(1)$).

2.1. Probe systems

TJ-II is fitted with a set of probe systems. There are two reciprocating probe drives, located at toroidal angles $\phi = 38.2°$ (the D probe, entering the plasma from above) and at $\phi = 195°$ (the B probe, entering the plasma from below). Each drive can be fitted with different probe heads. In the experiments discussed here, the D probe was fitted with a two-dimensional probe head (with 4×5 pins laid out in a poloidal-radial grid), while the B probe was fitted with a rake probe head (with 12 pins laid out in a radial array). For more details, please refer to [9].

In view of the following, we remark on the issue of the precision of the probe position and the magnetic configuration. The location of the probe has been carefully calibrated with respect to the vacuum vessel of TJ-II, yielding a precision of 1–2 mm. The precision of the construction of the coil system leads to a certain precision of the magnetic configuration, leading to errors of up to around 6 mm [10]. Finally, the presence of finite currents inside the plasma may move the rational surfaces of the magnetic configuration slightly [11]. In the present experiments, the currents were kept small ($|I_p| < 0.5$ kA) and the region of interest is near the plasma edge, where current-induced displacements of the rational surfaces are smallest. Overall, the displacement of the nominal probe position with respect to the calculated (vacuum) magnetic surfaces may amount up to about 1 cm.

2.2. Resistive MHD model

The model used for the present calculations is a MHD turbulence model which has been used in the past to interpret some experimental results from the TJ-II [12, 13] and W7-X [14] stellarators. It is based on the reduced MHD equations [15]. In the case of stellarators the dominant instability is the resistive pressure gradient driven instability. The magnetic geometry is that of a periodic cylinder, with minor radius a and length $L = 2\pi R_0$. We use a coordinate system (r, θ, ζ), in which r is the radius of the cylindrical surface, θ is the poloidal angle, and $\zeta = z/R_0$, where z is the coordinate along the axis of

the cylinder, so ζ is an effective toroidal angle when the cylinder is bent in a torus. The magnetic field line curvature κ includes the averaged effect of the toroidal and helical components of the magnetic field and is given by

$$\kappa \equiv \frac{r}{R_0} B_0^2 V''.$$

Here, the prime denotes the derivative with respect to toroidal flux, and $V' = \int dl/B$ is the specific volume enclosed by a flux surface.

The four equations of the model are summarized here in their dimensionless form,

$$\frac{\partial \tilde{\psi}}{\partial t} = \nabla_\parallel \Phi - S\bar{\omega}_{*e}\left(\frac{T_{eq}}{n_{eq}}\nabla_\parallel n + \nabla_\parallel T_e\right) + \eta \tilde{J}_\parallel, \tag{1}$$

$$\frac{\partial \tilde{U}}{\partial t} = -\mathbf{v}_\perp \cdot \nabla U + S^2 \nabla_\parallel J_\parallel - S^2 \frac{\beta_0}{2\varepsilon^2}\kappa\left(\frac{T_{eq}}{n_{eq}}\frac{1}{r}\frac{\partial \tilde{n}}{\partial \theta} + \frac{1}{r}\frac{\partial \tilde{T}_e}{\partial \theta}\right) + \mu \nabla_\perp^2 \tilde{U}, \tag{2}$$

$$\frac{\partial \tilde{n}}{\partial t} = -\mathbf{v}_\perp \cdot \nabla n + \frac{S}{\bar{\omega}_{ci}}\nabla_\parallel J_\parallel + D_\perp \nabla_\perp^2 \tilde{n}, \tag{3}$$

$$\frac{\partial \tilde{T}_e}{\partial t} = -\mathbf{v}_\perp \cdot \nabla T_e + \frac{S}{\bar{\omega}_{ci}}\frac{T_{eq}}{n_{eq}}\nabla_\parallel J_\parallel + \chi_\perp \nabla_\perp^2 \tilde{T}_e + \nabla_\parallel\left(\chi_\parallel \nabla_\parallel T_e\right). \tag{4}$$

The first equation describes the evolution of the poloidal magnetic flux ψ, is derived from Faraday's and Ohm's laws. The second one is the momentum balance equation where U is the z component of the vorticity. The other two equations give the evolution of density n and electron temperature T_e. All quantities appearing in equations (1)-(4) are decomposed in an equilibrium component f_{eq} and a fluctuating component $\tilde{f}$, so $f = f_{eq} + \tilde{f}$.

A detailed description of the parameters and their values for the present numerical results can be found in Ref. [13]. Here, we use the results of the calculations for the TJ-II magnetic configuration labelled 100_44.

2.3. Intermittence

In this article, we use the methods for calculating the intermittence of temporal signals described in Refs. [16, 17, 3], which we summarize here for convenience. Given a time series $X = \{x_i, i = 1, \ldots, N\}$ that has been sampled at a constant sampling rate, we calculate the measure

$$\epsilon(1, i) = \frac{(x_i - \langle x_i \rangle)^2}{\langle (x_i - \langle x_i \rangle)^2 \rangle}, \qquad i = 1, \ldots, N, \tag{5}$$

where $\langle x_i \rangle = (\sum_{i=1}^{N} x_i)/N$. This measure can be averaged over subblocks of data of length $n < N$, as follows:

$$\epsilon(n, i) = \frac{1}{n}\sum_{j=0}^{n-1} \epsilon(1, i + j). \tag{6}$$

We then calculate the $\mathfrak{q}$-moments, $\langle \epsilon(n, i)^{\mathfrak{q}} \rangle$. In a given range of n-values, these moments are expected to scale like [18]:

$$\langle \epsilon(n, i)^{\mathfrak{q}} \rangle \propto n^{-K(\mathfrak{q})}, \tag{7}$$

where $K(1) \equiv 0$. If the time series X is monofractal, the function $K(\mathfrak{q})$ is asymptotically linear in $\mathfrak{q}$, otherwise the series is multifractal. The parameter $C(\mathfrak{q})$ is defined as [18]:

$$C(\mathfrak{q}) = \frac{K(\mathfrak{q})}{\mathfrak{q} - 1}. \tag{8}$$

Of special interest is the so-called "intermittence parameter" $C(1)$, which must be calculated as

$$C(1) = \left. \frac{dK(\mathfrak{q})}{d\mathfrak{q}} \right|_{\mathfrak{q}=1} \tag{9}$$

due to the singularity of Eq. 8 at $\mathfrak{q} = 1$. Its value ranges from 0, for a monofractal time series, to 1.

In the field of fusion, intermittence has mostly been studied on the basis of a different though related quantifier: the so-called 'flatness factor', equal to $F = K - 3$, where K is the kurtosis of the probability distribution function of the time series X [19, 20]. However, the 'flatness factor' is a time-averaged quantity and only an approximate indicator of intermittence [21], which is a concept that fundamentally refers to temporal variations, and is therefore better captured by the parameter $C(1)$ introduced above.

2.4. Interpretation of the intermittence parameter

The interpretation of the intermittence parameter $C(1)$ used here is mainly based on a recent study [4].

Turbulence in a magnetically confined fusion plasma includes helical modes that may be resonant on specific rational surfaces. The eigenfunction Φ of such a resonant helical mode may be either odd or even in radius r with respect to the resonant surface at $r = r_s$. Even modes will have the largest amplitude at $r = r_s$, while odd modes will peak slightly off the resonant surface. Where a single helical mode is dominant, and plasma flows are unimportant, the resulting fluctuations are essentially monofractal, hence $C(1)$ approximates zero.

The turbulence may drive zonal flows, preferentially occurring near, but not at, the mentioned resonant surfaces. This poloidal flow mixes the local temporal fluctuations of the helical mode with its poloidal structure, leading to fluctuations with a multifractal character. A radial electric field will have a similar effect, as it will induce poloidal rotation.

Another cause for loss of monofractality may be the density of resonant helical modes: if this density is high (i.e., the resonant surfaces are close together due to, e.g., high magnetic shear), the corresponding modes may overlap, also inducing multifractal behavior. This happens normally close to the plasma edge where the magnetic shear tends to be large so that rational surfaces are close together. Correspondingly, in the plasma edge region the structure of turbulence is typically multifractal [4]. This situation also suggests that it may be easier to detect radial minima of $C(1)$ in low-

shear stellarators, where the resonant helical surfaces tend to be spaced farther apart than in, e.g., tokamaks.

So, in summary, fluctuations will tend to be monofractal only near low-order rational surfaces, where a single helicity is dominant, in the absence of poloidal flows and interference from other nearby resonances. Therefore, under specific conditions, minima of $C(1)$ can be used to localize some important low-order rational surfaces.

3. Rotational transform scan experiments

We performed a series of dynamic configuration scans in low density ECR heated plasmas (nominal power: 2×250 kW) by varying the rotational transform at the edge, $\iota(1) = \iota(1)/2\pi$, slowly and linearly in time (by modulating the external coil currents), while using plasma current control to keep currents inside the plasma small ($|I_p| < 0.5$ kA). Due to the low current and low plasma pressure ($\beta < 0.1\%$), Shafranov shifts of the flux surfaces are insignificant [22]. Thus, the magnetic configuration is very tightly controlled, particularly in the external part of the plasma, $\rho = r/a > 0.8$, where the influence of plasma currents on the magnetic configuration is weak [5]. Table 1 shows the 5 scans that were performed, while Fig. 1 shows the corresponding ι profiles. The shape of the ι profiles is very similar except for an offset.

The first 4 scans were made at low line average electron density ($\overline{n_e} < 0.6 \cdot 10^{19}$ m^{-3}), so that the plasma is in the Neoclassical electron root, in which the radial electric fiel E_r is predominantly positive throughout the plasma [23]. The fifth scan consists of a number of discharges in which $\overline{n_e}$ was gradually raised from about 0.4 to about $0.75 \cdot 10^{19}$ m^{-3}, crossing the critical density at around $0.6 \cdot 10^{19}$ m^{-3} and passing from electron to ion root. This change in confinement state is characterized by a change of sign of the radial electric field, E_r, specifically in the edge region of the plasma.

Table 1. Main characteristics of the configuration scans discussed here. The linear scans occur between $t = 1100$ ms and $t = 1250$ ms.

Scan number	Start configuration	End configuration	Start $\iota(1)/2\pi$	End $\iota(1)/2\pi$	Nr. discharges
1	100_46_65	101_42_64	1.672	1.630	10
2	101_42_64	100_46_65	1.630	1.672	5
3	101_42_64	101_38_62	1.630	1.593	10
4	101_38_62	101_42_64	1.593	1.630	10
5	101_38_62	101_42_64	1.593	1.630	21

The interpretation of the experimental results is facilitated by comparing them with calculations made using a resistive MHD turbulence model that has provided useful insights in the past (see Section 2). The model performs turbulence simulations in a simplified cylindrical geometry, but with profiles of density, temperature, and rotational transform similar to the experimental situation. Once the numerical calculation reached steady state, we then extracted temporal data of the fluctuating plasma potential at specific spatial points, which can be thought of as 'synthetic Langmuir probes'.

Performing a rotational transform scan similar to that of the experiment is very expensive, as in that case a new turbulence simulation run must be performed for each choice of rotational transform. So, instead, we took a single numerical calculation and moved the synthetic probes radially though the plasma. One should bear in mind that

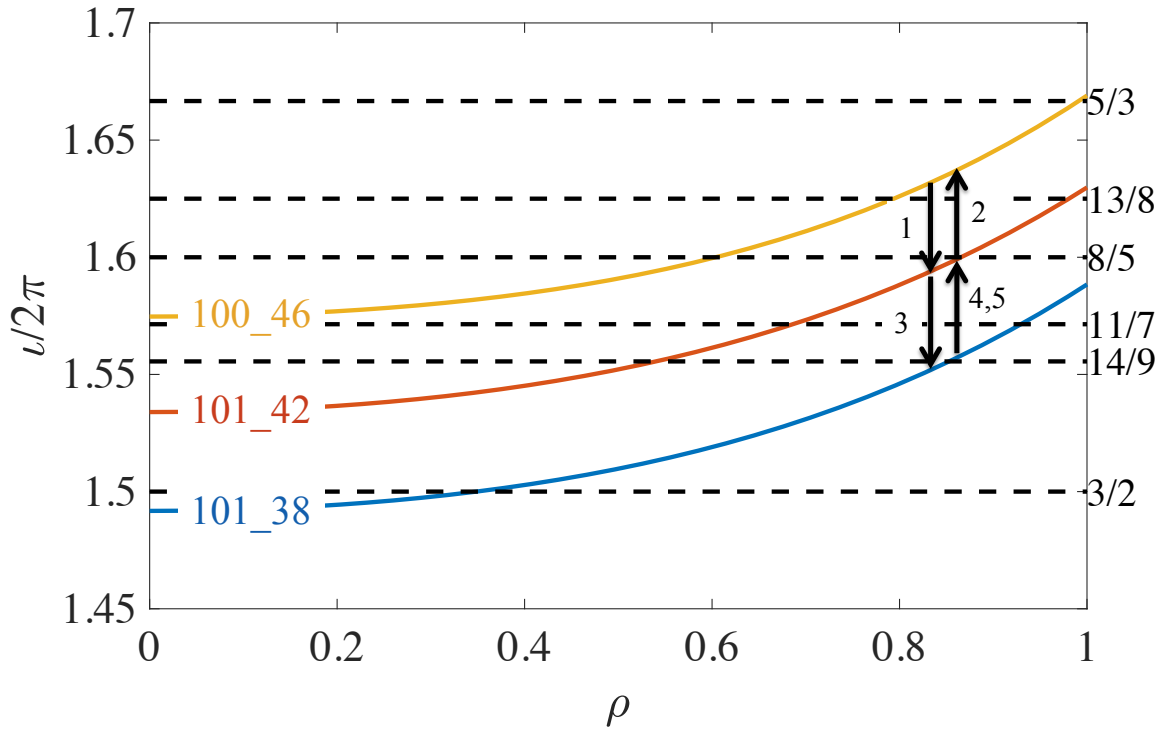

Figure 1. The rotational transform, $\iota/2\pi$, for various relevant configurations (labelled by the first two numbers of the configuration labels of Table 1). Some rational values of $\iota/2\pi$ are indicated by means of horizontal dashed lines. The 5 scans are indicated symbolically with black arrows.

this implies that the gradients of the density and temperature profiles are not constant at the probe locations, but vary according to the radial positions of the synthetic probes, which is an important difference with the experimental situation. Correspondingly, this approach prevents us from precisely reproducing the experimental values of the intermittence parameter, but helps us understand the observed radial structure of maxima and minima.

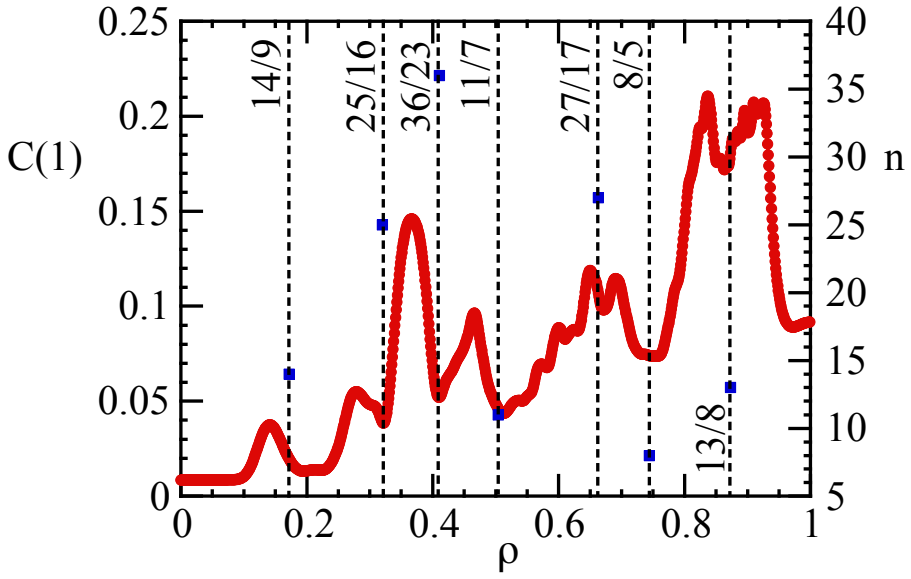

Figure 2. Intermittence parameter, $C(1)$, calculated from turbulence simulation using the resistive MHD model. Some low order rationals are indicated (the n value of the rationals n/m is indicated with blue squares, corresponding to the right axis).

3.1. Intermittence in electron root plasmas

We performed a numerical calculation using the resistive MHD model in configuration 100_44_64 (halfway between the endpoints of the scans of Table 1). We ran the simulation until steady state was obtained and then continued until we obtained sufficient data in the steady state phase to apply the multifractal analysis to the various fluctuating quantities. Fig. 2 shows the intermittence parameter for the potential fluctuations, C(1), as a function of radius. The intermittence parameter shows minima at various low order rational surfaces, consistent with results obtained in previous work [4] for electron temperature fluctuations. This simulation result provides a guide for the analysis of experimental results in the following.

From the floating potential measured with one of the probes (probe D) in TJ-II, we compute the intermittence parameter $C(1)$ (cf. Section 2). In the following, we assume that the effect of electron temperature fluctuations is small, so that the results for the experimental floating potential may be compared to the results for the plasma potential from the simulation. Fig. 3 shows the value of $C(1)$ versus ι at the nominal position of the probe, ρ. To estimate ι at the nominal position of probe D, we use the expression $\iota(\rho) = 0.165 + 0.879\iota(1)$, deduced from Fig. 2 of [5].

From previous work [4], we expect that the main low-order rational produces a clear minimum in the intermittence parameter $C(1)$. Considering that the uncertainty in the

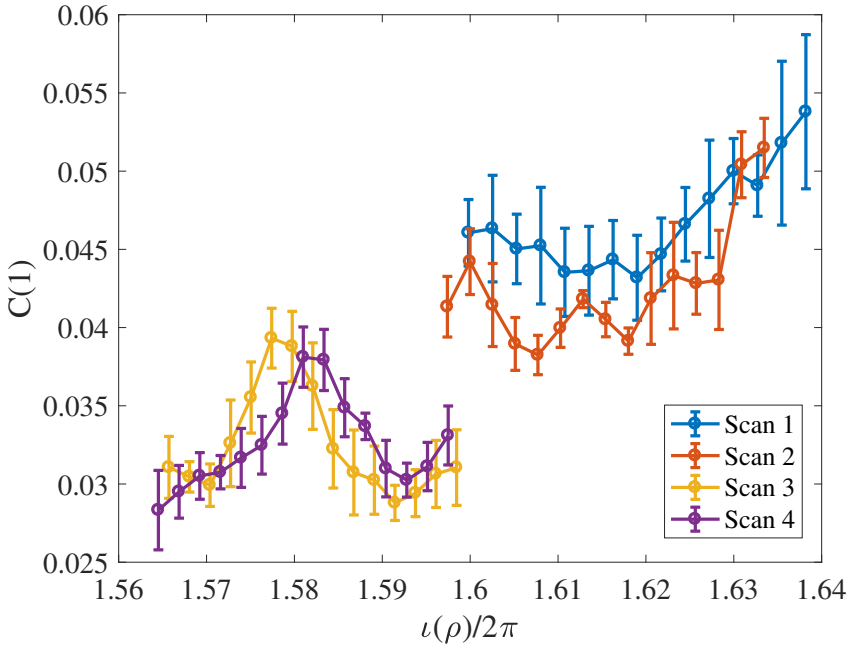

Figure 3. Intermittence parameter, $C(1)$, calculated from a Langmuir probe signal in the experiments. The abscissa shows the estimated rotational transform at the nominal probe positions (uncorrected, see text).

probe position (≤ 1 cm) corresponds to an error in ι of up to about 0.01 at the probe location, it seems likely that the minimum observed to occur at $\iota \simeq 1.592$ corresponds, in fact, to $\iota = 1.6$, implying that the nominal ι should be corrected by adding 0.008.

After applying this correction, we compare the experimental result for the intermittence parameter to the result obtained from the model, as shown in Fig. 4. This figure also indicates the location of a few important low order rational surfaces. Although the ordinates corresponding to the two curves are different, nevertheless the agreement of the general behavior is rather striking. The experimental and model curves for $C(1)$ do not only match regarding the main minimum at $\iota = 1.6$, but also with respect to the general trend (between $\iota = 11/7$ and $13/8$) and the secondary minimum near $\iota = 21/13$. The drop of the $C(1)$ curve of the model for $\iota > 1.63$ is a boundary effect of the simulation. The difference in amplitude of the two curves can be explained from the fact that the numerical calculation does not model the full process of the changing external currents (i.e., the magnetic configuration), nor the fact that the experimental electron density is roughly constant at the fixed measurement points. In the numerical calculation, the whole plasma is kept in a fixed state, with radially varying electron density. Furthermore, the experimental data may of course be affected by noise and other instrumental effects.

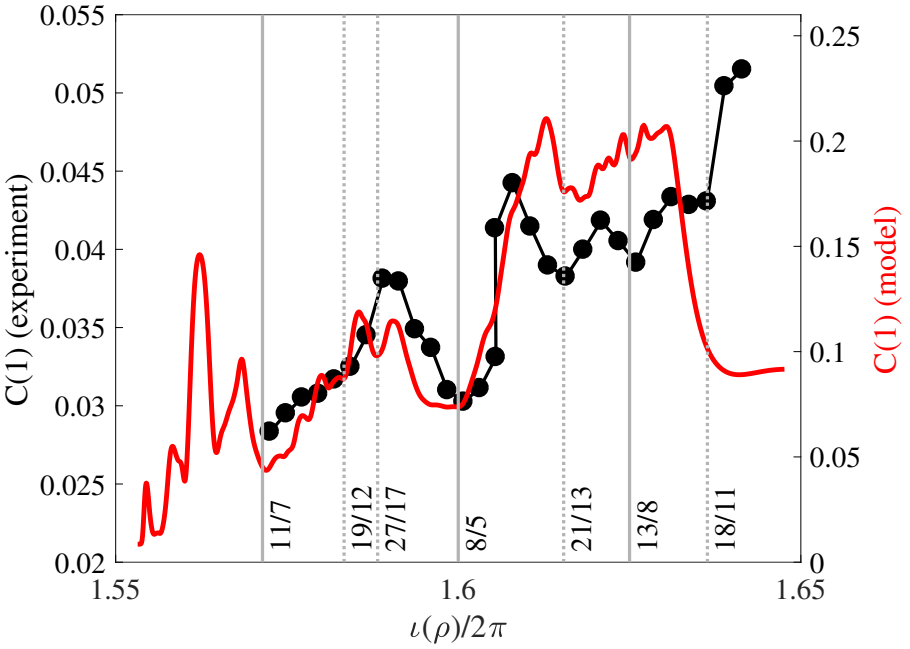

Figure 4. Intermittence parameter, $C(1)$, calculated from a Langmuir probe signal in the electron root rotational transform scan scan experiments, compared to the modeling result. The experimental data are identical to those of scans 2 and 4 shown in Fig. 3), but their rotational transform values have been corrected by the ad-hoc shift of +0.008, as motivated in the text.

3.2. Intermittence and change of root

We also applied the analyses of the preceding sections to the fifth scan of Table 1. This scan is similar to scan 4, except that the line averaged electron density, $\overline{n_e}$, was slowly raised on a shot by shot basis, while kept approximately constant in each discharge. Fig. 5 shows the variation of the line averaged density $\overline{n_e}$ and the radial electric field, E_r, in this series of shots. Here, E_r was estimated as the negative radial gradient of the floating potential at the probe, $-\nabla_r \phi_f$. The error bars indicate the standard deviation of the corresponding quantity, calculated from the variation in the relevant time window ($1100 \leq t \leq 1250$ ms). These graphs highlight the systematic density variation that was achieved in this series of shots, and the resulting gradual change in the mean radial electric field. Below and above the critical density at $\overline{n_e} \simeq 6.5 \cdot 10^{19}$ m^{-3}, the density was kept rather constant in time, leading to small values of the standard deviation, but near the critical density, spontaneous density variations were produced as a consequence of the fact that the plasma was close to the confinement transition (electron–ion root), leading to larger values of the standard deviation.

Fig. 6 shows the variation of the intermittence parameter and the radial electric field with line average density. Here, the correction of ι discussed above has been applied, so that the values of ι shown correspond, to good approximation, to the local values of ι at the measurement location.

As the density increases, so does the density gradient and the turbulence drive. Nevertheless, the turbulence does not necessarily increase everywhere, as the turbulence may locally produce zonal flows that break up the turbulent eddies [24].

We observe that the intermittence parameter gradually develops two clear local minima as the density rises. The first minimum appears close to the location of the most important low order rational surface in this range, $\iota = 8/5$. It is already present when $\overline{n_e} \simeq 0.45 \cdot 10^{19}$ m^{-3} and deepens as the density is raised. The second minimum, near the low order rational surface of $\iota = 27/17$, is absent at low density but becomes visible gradually for $\overline{n_e} \gtrsim 0.65 \cdot 10^{19}$ m^{-3}. We note also that this second minimum at 27/17 is apparent as a small dip in the theoretical curve shown in Fig. 4.

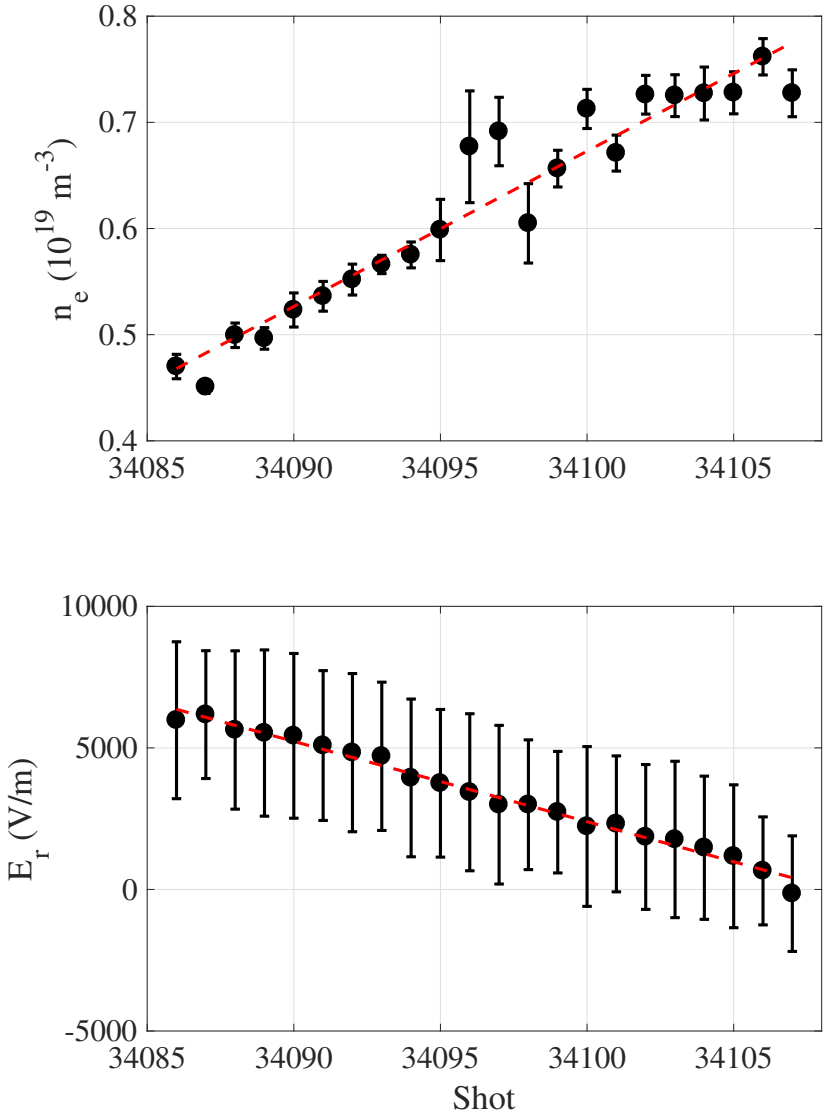

Figure 5. Mean line averaged electron density, $\overline{n_e}$ and radial electric field, E_r, and their standard deviations, for the discharges of scan 5 (cf. Table 1), as a function of shot number. In each discharge, the rotational transform is scanned as described in the text. The red dashed lines merely serve to guide the eye.

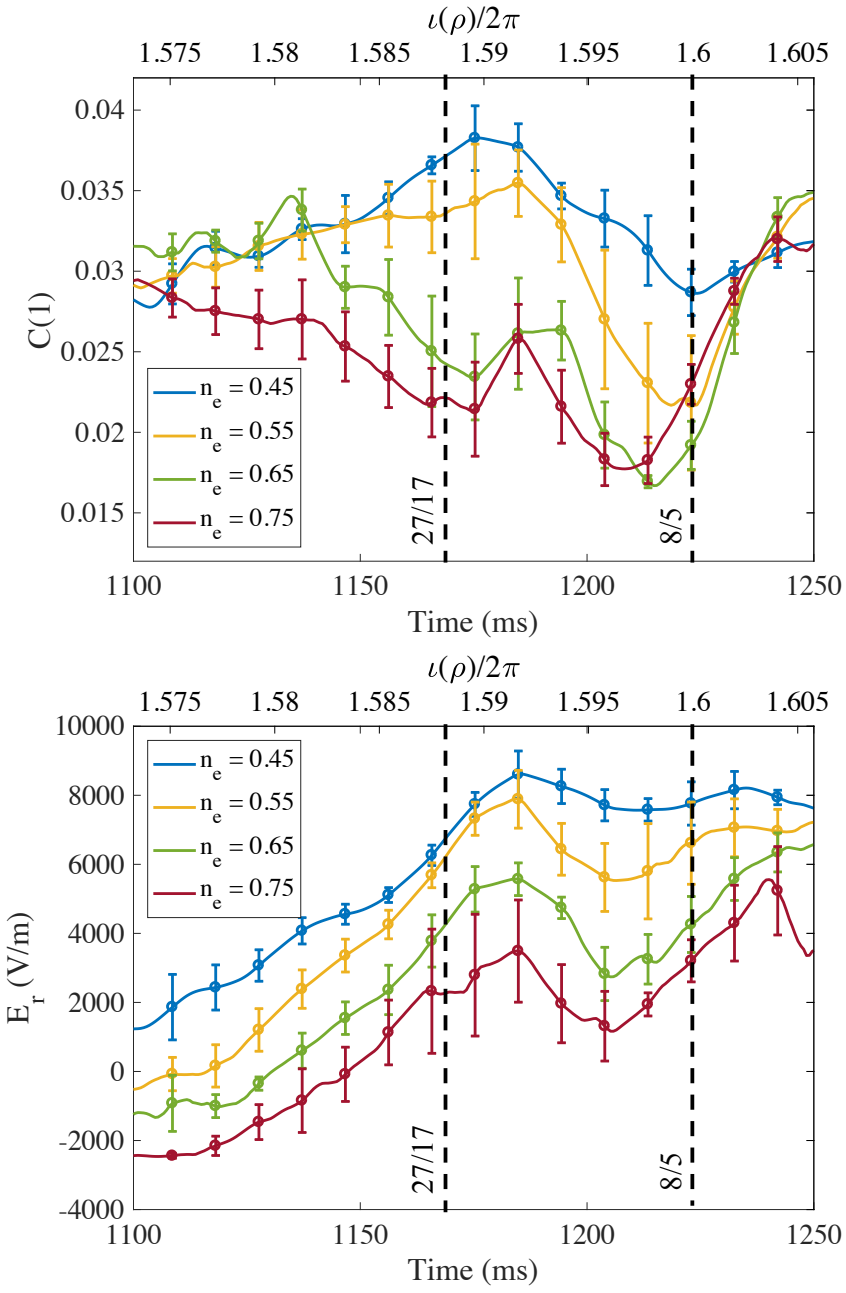

Figure 6. Profiles of (top) the intermittence parameter, $C(1)$, and (bottom) the radial electric field, E_r, as a function of $\overline{n_e}$ (indicated in the legends, in units of 10^{19} m^{-3}. Vertical dashed lines indicate the location of the 8/5 and 27/17 rational surfaces. Error bars indicate the experimental standard deviation in the corresponding density range (bins of width $0.1 \cdot 10^{19}$ m^{-3}, centered around the density values indicated in the legends).

3.3. Effect of E_r at constant density

Referring to Fig. 5, one observes that the last few discharges of the density scan have nearly constant density, whereas the radial electric field, E_r, continues to vary. This offers the opportunity to study the effect of E_r on the intermittence parameter at constant $\overline{n_e}$. It should be noted that the error bars shown indicate the standard deviation of these quantities over the rotational transform scan ($1100 \leq t \leq 1250$), not the measurement error, which is much lower.

In Fig. 7, we compare the profiles of E_r and $C(1)$ between shots 34100 and 34107, having a similar value of $\overline{n_e}$, but a rather different value of E_r. At low E_r (red dashed curves), a minimum can only be seen near the rational surface 8/5, and as E_r is increased (black continuous curves), the minimum at 8/5 deepens, while a new minimum near 27/17 appears. From these figures, we deduce that an increase of E_r leads to a decrease of $C(1)$ around the corresponding low order rational surfaces, but not elsewhere.

To study the effect of E_r in the simulation, the steady state turbulence calculations that underlie the results for the intermittence parameter shown in Fig. 2 were continued for an additional period of time in which a positive radial electric field was added. We then calculated the intermittence parameter for the potential fluctuations during this additional period. The effect of the radial electric field can be seen in Fig. 8 which shows the ratio of the curves of $C(1)$ with and without applied E_r. The figure shows that the application of positive poloidal $E \times B$ rotation reduces the intermittence parameter at the low order rational surfaces 8/5 and 25/13, making the minima deeper, so that the system becomes more monofractal at these positions. This can be explained from the fact that the intrinsic poloidal flow generated by the turbulence in the region of these resonances is negative, so that the added positive flow reduces the net poloidal rotation. Contrariwise, the preexisting intrinsic flow at the rational surface 13/8 is positive, so that adding a positive $E \times B$ rotation increases the flow at this location, resulting in the observed increase of $C(1)$. Thus, an imposed external flow may either reduce or increase the value of $C(1)$ near rational surfaces. These issues will be studied in more detail in future work.

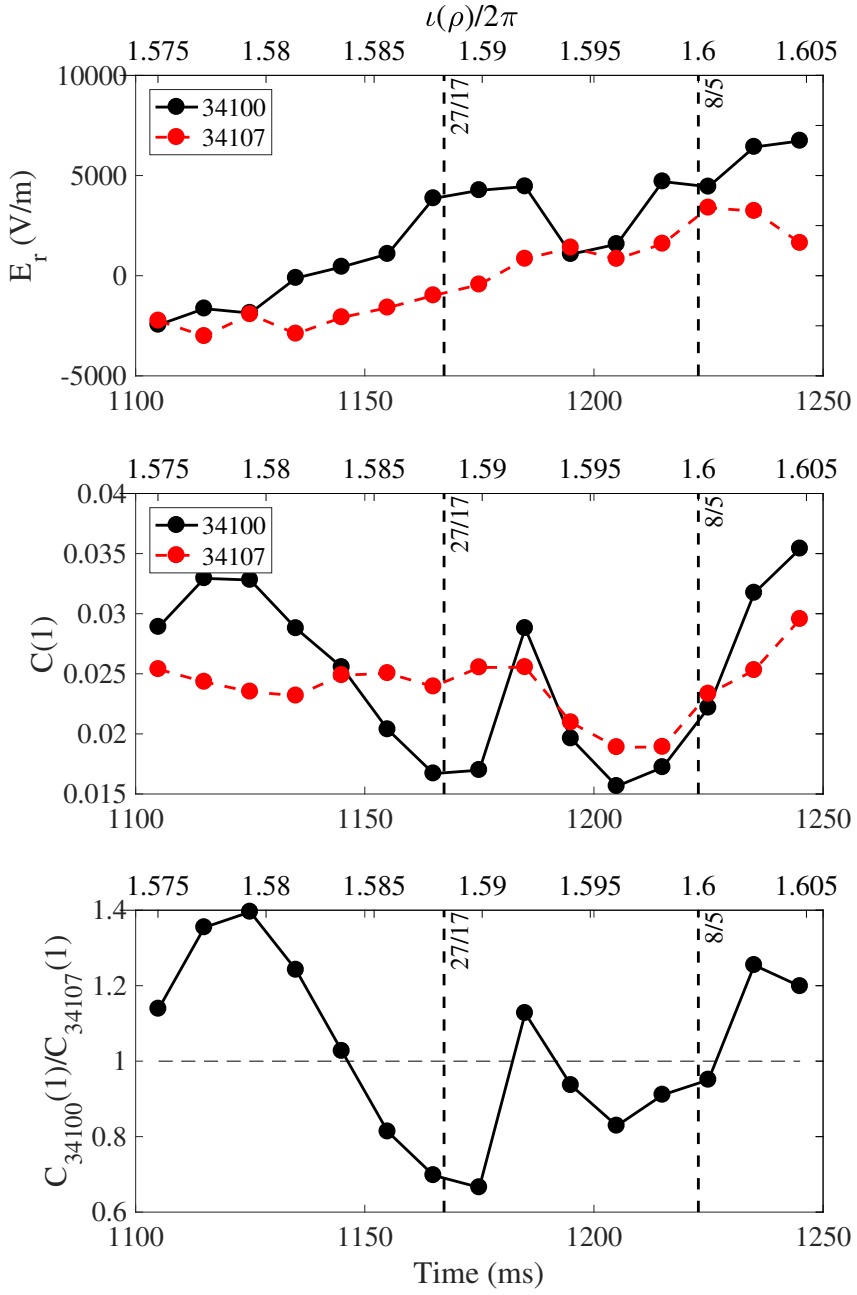

Figure 7. Profiles of (top) the radial electric field, E_r and (middle) the intermittence parameter, $C(1)$, for two selected discharges with a similar value of $\overline{n_e}$. Bottom: the ratio of the two curves of $C(1)$ shown, highlighting the change of intermittence due to a change in E_r only.

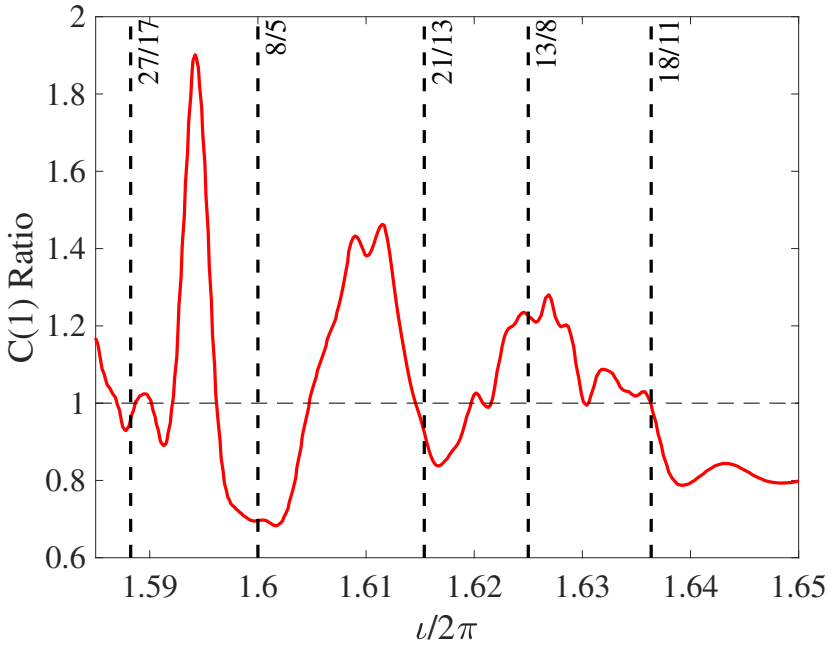

Figure 8. Ratio of intermittence parameter profiles after / before applying the radial electric field E_r in the resistive MHD model.

4. Discussion and conclusions

This paper addresses the use of the multifractal intermittence parameter [2] to obtain relevant information about turbulence and flows in the core plasma of magnetic confinement devices. The interpretation of this parameter is based on previous work [4] and summarized here in Section 2.4.

In this framework, we reanalyze a set of experiments involving careful dynamical scans of the rotational transform, ι, performed some years ago in the TJ-II stellarator [5]. The dynamical scans were performed in a narrow range of ι (cf. Fig. 1) over a time interval of 150 ms, while perturbative plasma currents were minimized to the best of our ability.

Using a fixed Langmuir probe in the edge region of the plasma (at $\rho \simeq 0.85$), we measured the floating potential and studied the evolution of the intermittence parameter $C(1)$ versus time, in subwindows of 10 ms, which could be transformed, with a minimum number of assumptions, to its evolution versus the local ι.

In a first set of experiments (Section 3.1), performed at low electron density in 'electron root' conditions, we observed variations of $C(1)$ with ι, revealing minima at the locations of important low order rational surfaces. When these results were compared to the intermittence produced by the resistive MHD turbulence calculation in similar conditions, very good agreement was obtained. The locations of 5 low order rational surfaces could be identified inside the plasma, an unparalleled feat in plasma physics, to the best of our knowledge.

In a second set of experiments (Section 3.2), we studied the variation of $C(1)$ as the line average density was raised on a shot by shot basis. In doing so, the TJ-II plasma performed a gradual confinement transition from 'electron' to 'ion root' and the radial electric field E_r changed sign from predominantly positive to slightly negative (cf. Fig. 5). As the density was raised, we found that the intermittence at the rational surfaces decreased, while it increased at other locations. A possible explanation is the increased drive (increased gradients) for instabilities, which would emphasize the monofractal properties at the rational surfaces, while increasing the generation of zonal flows and the associated mixing (leading to multifractality) away from the rational surfaces (noting that the effect low order rational surfaces have on the local radial electric field has been reported in previous work [25]). The reduction of intermittence at rational surfaces led to the detection of a new low order rational (27/17) that had not been identified in the first set of experiments, performed at low density.

A subset of discharges from the second set of experiments (Section 3.3), at nearly constant line averaged electron density, $\overline{n}_e$, allowed determining the specific effect of the radial electric field, E_r on the intermittence parameter. We found that an increased radial electric field decreases the intermittence at the considered rational surfaces. Again, the response of the intermittence to an added electric field is fully consistent with the results of numerical calculations using the resistive MHD model.

From the theoretical arguments given in Section 2.4 and the experimental results,

we conclude that the intermittence parameter is a powerful tool to detect the location of low order rational surfaces. When the turbulence drive is increased, the intermittence at a given rational surface may decrease (as increased turbulence would enhance monofractality at such locations). This is exemplified by the results shown in Section 3.2, where a new minimum corresponding to the rational 27/17 appeared when the driving gradient was raised. On the other hand, away from the low order rationals, the increased drive can lead to an enhancement of intermittence, presumably due to an increase in the generation of zonal flows and the associated mixing (leading to multifractality).

We emphasize that the minima of the intermittence parameter detected in the present work occur in a logical succession. The experimental range studied is $1.57 \leq \iota \leq 1.64$. The rational values n/m occurring in this range can be ordered according to increasing value of $n + m$, leading to the following series (restricted to $n \leq 27$ and listing only simplified fractions):

$$\left\{ \mathbf{\frac{8}{5}}, \mathbf{\frac{11}{7}}, \mathbf{\frac{13}{8}}, \frac{18}{11}, \frac{19}{12}, \mathbf{\frac{21}{13}}, \mathbf{\frac{27}{17}} \right\} \tag{10}$$

Here, we have marked the rationals that appeared as minima in our intermittence graphs in bold typeface. It is interesting to note that the lowest order rationals in the experimental range are detected systematically.

The results shown here are consistent with those of our previous work [4], which includes experimental results for the W7-X stellarator, in which a minimum of the intermittence parameter was observed to track the location of low order rationals as the rotational transform profile was scanned on a shot by shot basis.

As a side remark, we note that the present technique could be used at TJ-II to perform an absolute calibration of the Langmuir probe positions with respect to the magnetic geometry.

In summary, we propose that the intermittence parameter constitutes a unique new tool to detect low-order rational surfaces in fusion plasmas. Their correct identification may be an important step forward in our understanding of the impact of rational surfaces on confinement in fusion devices. The fact that TJ-II and W7-X are low shear stellarators may facilitate the application of this tool, although this is as yet unclear. Perhaps the technique can be fruitfully applied at other devices, such as tokamaks. Regardless, the study of intermittence may be helpful for the understanding of turbulence in general.

Acknowledgements

Research sponsored in part by the *Ministerio de Economía y Competitividad* of Spain under project Nr. ENE2015-68265-P and by the *Ministerio de Ciencia, Innovación y Universidades* of Spain under project Nr. PGC2018-097279-B-I00. This work has been carried out within the framework of the EUROfusion Consortium and has received funding from the Euratom research and training programme 2014-2018 and 2019-2020 under grant agreement No 633053. The views and opinions expressed herein do not necessarily reflect those of the European Commission.

References

[1] ITER Physics Expert Groups on Confinement and Transport and Confinement Modelling and Database et al. Chapter 2: Plasma confinement and transport. *Nucl. Fusion*, 39(12):2175, 1999. doi:10.1088/0029-5515/39/12/302.

[2] B.B. Mandelbrot. *Multifractals and* $1/f$ *noise*. Springer, 1998.

[3] B.A. Carreras, V.E. Lynch, D.E. Newman, R. Balbín, J. Bleuel, M.A. Pedrosa, M. Endler, B. van Milligen, E. Sánchez, and C. Hidalgo. Intermittency of plasma edge fluctuation data: Multifractal analysis. *Phys. Plasmas*, 7(8):3278, 2000. doi:10.1063/1.874193.

[4] B.A. Carreras, L. García, J.H. Nicolau, B.Ph. van Milligen, U. Hoefel, M. Hirsch, and the TJ-II and W7-X Teams. Intermittence and turbulence in fusion devices. *Plasma Phys. Control. Fusion*, 62:025011, 2020. doi:10.1088/1361-6587/ab57f9.

[5] B.Ph. van Milligen, A. Lopez Fraguas, M.A. Pedrosa, C. Hidalgo, A. Martín de Aguilera, and E. Ascasíbar. Parallel and perpendicular turbulence correlation length in the TJ-II stellarator. *Nucl. Fusion*, 53:093025, 2013. doi:10.1088/0029-5515/53/9/093025.

[6] J.H. Harris, J.L. Cantrell, T.C. Hender, B.A. Carreras, and R.N. Morris. A flexible heliac configuration. *Nucl. Fusion*, 25(5):623, 1985. doi:10.1088/0029-5515/25/5/005.

[7] Ch.P. Ritz, H. Lin, T.L. Rhodes, and A.J. Wootton. Evidence for confinement improvement by velocity-shear suppression of edge turbulence. *Phys. Rev. Lett.*, 65:2543, 1990. doi:10.1103/PhysRevLett.65.2543.

[8] C. Alejaldre, J. Alonso, L. Almoguera, E. Ascasíbar, A. Baciero, R. Balbín, M. Blaumoser, J. Botija, B. Brañas, E. de la Cal, A. Cappa, R. Carrasco, F. Castejón, J. R Cepero, C. Cremy, J. Doncel, C. Dulya, T. Estrada, A. Fernández, M. Francés, C. Fuentes, A. García, I. García-Cortés, J. Guasp, J. Herranz, C. Hidalgo, J.A. Jiménez, I. Kirpitchev, V. Krivenski, I. Labrador, F. Lapayese, K. Likin, M. Liniers, A. López-Fraguas, A. López-Sánchez, E. de la Luna, R. Martín, A. Martínez, M. Medrano, P. Méndez, K. McCarthy, F. Medina, B. van Milligen, M. Ochando, L. Pacios, I. Pastor, M.A. Pedrosa, A. de la Peña, A. Portas, J. Qin, L. Rodríguez-Rodrigo, A. Salas, E. Sánchez, J. Sánchez, F. Tabarés, D. Tafalla, V. Tribaldos, J. Vega, B. Zurro, D. Akulina, O. I Fedyanin, S. Grebenshchicov, N. Kharchev, A. Meshcheryakov, R. Barth, G. van Dijk, H. van der Meiden, and S. Petrov. First plasmas in the TJ-II flexible heliac. *Plasma Phys. Control. Fusion*, 41:A539, 1999. doi:10.1088/0741-3335/41/3A/047.

[9] B.Ph. van Milligen, J. Hernández Nicolau, B. Liu, G. Grenfell, U. Losada, B. Carreras, L. García, and C. Hidalgo. Filaments in the edge confinement region of TJ-II. *Nucl. Fusion*, 58:026030, 2018. doi:10.1088/1741-4326/aa9db6.

[10] E. Ascasíbar, J. Qin, and A. López-Fraguas. Magnetic surface mapping experiments in TJ-II heliac. *J. Plasma Fusion Res. SERIES*, 1:183, 1998.

[11] D. López-Bruna, F. Castejón, T. Estrada, J.A. Romero, J.A. Jiménez, E. Ascasíbar, and the TJ-II Team. Effects of ohmic current in the TJ-II stellarator. *Nucl. Fusion*, 44:645, 2004.

[12] L. García, B.A. Carreras, V.E. Lynch, M.A. Pedrosa, and C. Hidalgo. Sheared flow amplification by vacuum magnetic islands in stellarator plasmas. *Phys. Plasmas*, 8(9):4111, 2001. doi:10.1063/1.1392996.

[13] B.Ph. van Milligen, J.H. Nicolau, L. García, B.A. Carreras, C. Hidalgo, and the TJ-II Team. The impact of rational surfaces on radial heat transport in TJ-II. *Nucl. Fusion*, 57(5):056028, 2017. doi:10.1088/1741-4326/aa611f.

[14] B.Ph. van Milligen, U. Hoefel, J.H. Nicolau, M. Hirsch, L. García, B.A. Carreras, C. Hidalgo, and the W7-X Team. Study of radial heat transport in W7-X using the transfer entropy. *Nucl. Fusion*, 58(7):076002, 2018. doi:10.1088/1741-4326/aabf5d.

[15] H.R. Strauss. Nonlinear, three-dimensional magnetohydrodynamics of noncircular tokamaks. *Phys. Fluids*, 19:134, 1976. doi:10.1063/1.861310.

[16] C. Meneveau and K.R. Sreenivasan. Simple multifractal cascade model for fully developed turbulence. *Phys. Rev. Lett.*, 59:1424, 1987. doi:10.1103/PhysRevLett.59.1424.

[17] C. Meneveau and K.R. Sreenivasan. The multifractal nature of turbulent energy dissipation. *J. Fluid Mechanics*, 224:429, 1991. doi:10.1017/S0022112091001830.

[18] H.G.E. Hentschel and I. Procaccia. The infinite number of generalized dimensions of fractals and strange attractors. *Physica D*, 8(3):435, 1983. doi:10.1016/0167-2789(83)90235-X.

[19] G.Y. Antar, P. Devynck, X. Garbet, and S.C. Luckhardt. Turbulence intermittency and burst properties in tokamak scrape-off layer. *Phys. Plasmas*, 8(5):1612, 2001. doi:10.1063/1.1363663.

[20] V. Carbone, G. Regnoli, E. Martines, and V. Antoni. Intermittency and self-similarity in plasma edge fluctuations. *Phys. Plasmas*, 7(2):445, 2000. doi:10.1063/1.873828.

[21] V.A. Sandborn. Measurements of intermittency of turbulent motion in a boundary layer. *J. Fluid Mechanics*, 6(2):221, 1959. doi:10.1017/S0022112059000581.

[22] B.Ph. van Milligen, T. Estrada, E. Ascasíbar, D. Tafalla, D. López-Bruna, A. López-Fraguas, J.A. Jiménez, I. García-Cortés, A. Dinklage, R. Fischer, and the TJ-II Team. Integrated data analysis at TJ-II: the density profile. *Rev. Sci. Instrum.*, 82(7):073503, 2011. doi:10.1063/1.3608551.

[23] J.L. Velasco, J.A. Alonso, I. Calvo, and J. Arévalo. Vanishing neoclassical viscosity and physics of the shear layer in stellarators. *Phys. Rev. Lett.*, 109(13):135003, 2012. doi:10.1103/PhysRevLett.109.135003.

[24] H. Biglari, P.H. Diamond, and P.W. Terry. Influence of sheared poloidal rotation on edge turbulence. *Phys. Plasmas*, 2:1, 1990. doi:10.1063/1.859529.

[25] O. Bondarenko, T. Estrada, R. Jiménez-Gómez, D. López-Bruna, T. Happel, J. Romero, A. López-Fraguas, E. Ascasíbar, and E. Blanco. Influence of low order rational surfaces on the radial electric field of TJ-II ECH plasmas. *Contrib. Plasma Phys.*, 50(6-7):605, 2010.